Phase coherence of charge-6e superconductors with a frustrated Kagome XY antiferromagnet

Feng-Feng Song(宋峰峰)[1] and Guang-Ming Zhang(张广铭)[2,3,4*]

[1]*Institute for Solid State Physics, The University of Tokyo, Kashiwa, Chiba 277-8581, Japan*
[2]*State Key Laboratory of Low Dimensional Quantum Physics and Department of Physics, Tsinghua University, Beijing 100084, China*
[3]*School of Physical Science and Technology, ShanghaiTech University, Shanghai 201210, China*
[4]*Frontier Science Center for Quantum Information, Beijing 100084, China*

(Received 25 December 2024; accepted manuscript online 31 January 2025)

Recent experimental evidence of the charge-6e condensed phase in Kagome superconductors has generated significant interest. This study investigates the unconventional superconductivity in the Kagome superconductor CsV_3Sb_5, focusing on the emergence of charge-6e superconductivity (SC) at temperatures higher than the conventional charge-2e SC state. By modeling the phase coherence of the SC order parameter using a frustrated antiferromagnetic XY model on an emergent Kagome lattice, the condensation of fractional vortices with 1/3 vorticity stabilizes the phase coherence in $\exp(i3\theta)$, resulting in a charge-6e SC state. Using a tensor network approach tailored for frustrated spin systems, a Berezinskii-Kosterlitz-Thouless transition is identified at $T_c/J \simeq 0.075$, where the unbinding of 1/3 fractional vortex-antivortex pairs transforms the system from the charge-6e SC phase to the normal phase. Below T_c, the 1/3 fractional vortex correlations exhibit a power-law decay, whereas the integer vortex correlations decay exponentially, reflecting the dominance of charge-6e SC in the absence of charge-2e SC. The results provide a theoretical understanding of charge-6e SC in two-dimensional Kagome superconductors, emphasizing the interaction between fractional vortices, frustration, and topology in stabilizing the exotic SC phase.

DOI: 10.1088/0256-307X/42/3/037401 CSTR: 32039.14.0256-307X.42.3.037401

Introduction. The Kagome lattice, with its frustrated corner-sharing triangular geometry, has emerged as a versatile platform for studying the interaction between the nontrivial band topology, strong correlations, and intertwined electronic orders. Its distinctive features, including flat bands, van Hove singularities, and the potential to host quantum spin liquids, have been widely explored.[1–5] Among the Kagome-based materials, quasi-two-dimensional (2D) superconductors AV_3Sb_5 (A = K, Rb, Cs) have attracted significant attention because of their unconventional charge density wave (CDW) states above the subsequent superconductivity (SC) at low temperatures.[6–13] The CDW state in AV_3Sb_5 exhibits unconventional symmetry breaking properties, including spontaneous time-reversal symmetry breaking (TRSB)[6,14,15] and rotational symmetry breaking,[16,17] suggesting a complex interaction of electronic orders.

Recently, CsV_3Sb_5 has emerged as a promising platform for the study of unconventional SC. Magnetotransport experiments revealed an exotic SC phase diagram, including evidence of charge-6e SC in the strongly fluctuating region above the conventional charge-2e condensate.[18] A hallmark of charge-6e SC is the fractional magnetic flux quantization of $\frac{h}{6e}$, which distinguishes it from the usual charge-2e SC described by the Bardeen-Cooper-Schrieffer (BCS) theory. Charge-6e SC has been proposed to arise as a vestigial higher-order condensation of the bound states of electron sextets, possibly driven by strong fluctuations in the pair density wave (PDW) order.[19–23] In recent experiments, a commensurate 3$\boldsymbol{Q}$ PDW order, where the SC order parameter spatially modulated along three distinct directions, was observed in the SC state of CsV_3Sb_5,[17,24,25] suggesting the intricate intertwining of SC and PDW as a potential mechanism for the emergence of charge-6e SC.

Despite the significant theoretical progress in recent studies,[20,22] the physical origin and implications of the remarkable observations of charge-6e SC are not fully understood. To uncover the unconventional aspects of charge-6e SC and the role of the underlying frustrated Kagome geometry, it is crucial to understand the phase transitions associated with the SC order parameter of the PDW state. To capture the essential physics, this study focuses on the phase coherence of Cooper pairs, assuming that the amplitude fluctuations of the order parameter are frozen at low temperatures.[26–28] The analysis in this study shows that the phase coherence of the SC order parameter can be effectively described using a frustrated XY model of an emergent Kagome lattice that shares the same ground-state structure and topological excitations as the original system.[29–33] With this correspondence, magnetoresistance oscillations with a period of $\frac{h}{6e}$ can be naturally

*Corresponding author. Email: gmzhang@tsinghua.edu.cn
© 2025 Chinese Physical Society and IOP Publishing Ltd. All rights, including for text and data mining, AI training, and similar technologies, are reserved.

understood to arise from the condensation of 1/3 fractional vortex-antivortex pairs.

Using recently developed tensor network (TN) methods for frustrated spin systems,[34–37] this study determines the phase structure of the antiferromagnetic (AF) XY model with nearest-neighbor (NN) interactions on Kagome lattices. From the singularity of the entanglement entropy of the 1D quantum transfer operator, clear evidence of a single Berezinskii-Kosterlitz-Thouless (BKT) phase transition[38–40] is found, driven by the unbinding of fractional vortex-antivortex pairs with 1/3 vorticity. In the low-temperature phase, a quasi-long-range order (QLRO) is found in the spin variable $\exp(i3\theta)$, whereas the phase coherence of the integer vortices is destroyed, as indicated by the exponential decay of $\exp(i\theta)$ in the correlation functions. This clarified phase structure demonstrates a scenario in which the conventional charge-2e SC arising from Cooper pairs is suppressed, and an unconventional charge-6e SC state formed by the bound states of Cooper sextuples emerges as the dominant order.

AF Kagome XY Model. As the microscopic interaction was unknown, the simplest commensurate $3\boldsymbol{Q}$ complex PDW order parameter allowed by the $P6/mmm$ space group was considered:[20,23]

$$\Delta_{\rm pdw}(\boldsymbol{r}) = \Delta e^{i\theta} \sum_{\eta=1}^{3} e^{i2(\eta-1)\pi/3} \cos(\boldsymbol{Q}_\eta \cdot \boldsymbol{r} + \phi_\eta), \quad (1)$$

where Δ is the amplitude, θ is the global SC phase, $\boldsymbol{Q}_\eta$ are the modulation wave vectors, and the relative phases between the different modes were $\phi_\eta = 0$.

The spatial distributions of the PDW order parameters are shown in Fig. 1(a), where the amplitude is represented by the color intensity and the phase is indicated by arrows. The amplitude reached its minimum at the centers of the triangles and hexagons, whereas its maximum formed an emergent Kagome lattice. Consequently, the phase coherence of the order parameter was described effectively using the XY spin model, as shown in Fig. 1(b), where each spin corresponded to a phase angle at the maximum amplitude.

The phase distribution in Fig. 1(b) represents a massive degenerate ground-state of the AF XY model on the Kagome lattices,

$$H = J \sum_{\langle i,j \rangle} \cos(\theta_i - \theta_j), \quad (2)$$

where $J > 0$ and the sum run over all NNs. In addition to the overall $U(1)$ degrees of freedom (DoF), the frustration within each triangular plaquette induced chiral DoF. To minimize the energy, the three XY spins in a triangle must differ by an angle of $2\pi/3$, rotating either clockwise or counterclockwise. This assigns a chirality to each plaquette $\tau_i = \pm 1$. The extensive degeneracy of these chiralities can be mapped to a three-state AF Potts model with a residual entropy of $1.26k_{\rm B}$ per site.[41] This degeneracy results from the excitation of the zero-energy domain walls, as shown by the dotted orange line in Fig. 1(b) along with the permutation of the green and blue spins in the upper plane.

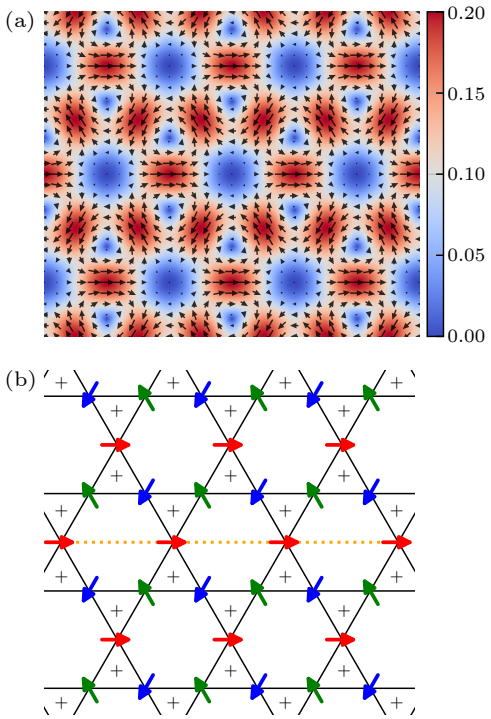

Fig. 1. (a) Spatial distribution of the complex PDW order parameter, with the amplitude represented by the color intensity and phase denoted by arrows. (b) Phase distribution of the PDW state on the emergent Kagome lattice represented by XY spins as a ground state of the AF XY model with chirality $\tau_i = +1$ on each triangular plaquette. The dotted orange line denotes a possible method for exciting a zero-energy domain wall.

The ferromagnetic ordering of chirality in the PDW state can be stabilized by a small AF next-to-nearest-neighbor (NNN) interaction, corresponding to a charge-2e SC state. The freezing of the chiral DoF was due to the finite energy of the domain walls.[32] However, as the temperature increased, the energy barrier was overcome, allowing the domain walls to proliferate and destroy the long-range chiral order. As the phase angles of the spins across a domain wall can change by $\pm 2\pi/3$, these chirality fluctuations allow the phase angle between distant spins to vary freely by multiples of $2\pi/3$. Such fluctuations increase with distance, destroying the QLRO of the XY spins of $\exp(i\theta)$ and leaving charge-6e in a vestigial state at higher temperatures, where $\exp(i3\theta)$ remains algebraic under $\pm 2\pi/3$ phase fluctuations.

Excitations of 1/3 Fractional Vortices. In the absence of chiral order, the concept of excess charges offers a clearer physical picture than complex domain wall configurations.[42] The topological charge of a vortex at the center of a hexagon is determined by the chiralities of the six surrounding triangles $q_{\rm h} = \frac{1}{3}\sum_{t=1}^{6} q_t$, where $q_t = \pm\frac{1}{2}$ corresponds to chiralities $\tau_t = \pm 1$. The relationship between the vortex charges and chirality configurations is shown in Fig. 2(b). An alternative set of vortex configurations can be generated by inverting all chiralities on the triangles. Integer vortex excitations do not disrupt the constraint that each spin must differ from its neighbors by $2\pi/3$

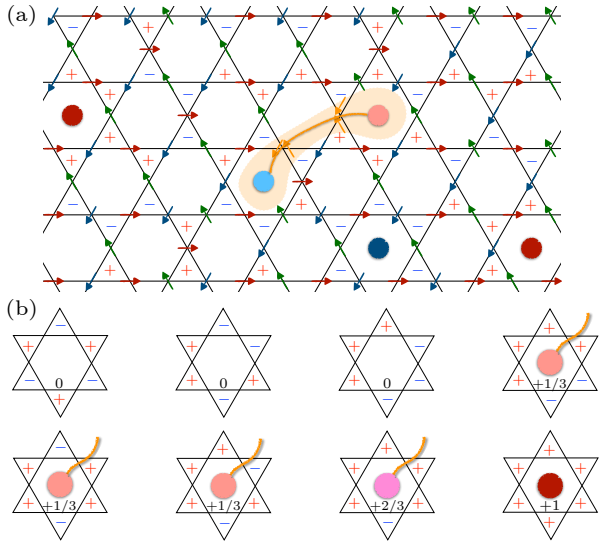

Fig. 2. (a) Bound pair of 1/3 vortices (red and blue circles) connected by a topological string (orange line) is formed by switching the chiralities of two adjacent triangles in one of the degenerate ground-state configurations. Integer vortices (dark red and blue circles) can freely excite. (b) Topological charges of vortices corresponding to different domain wall structures. A corresponding set of negative vortices can be obtained by inverting all chirality signs. Phase mismatches between spins are indicated by orange lines.

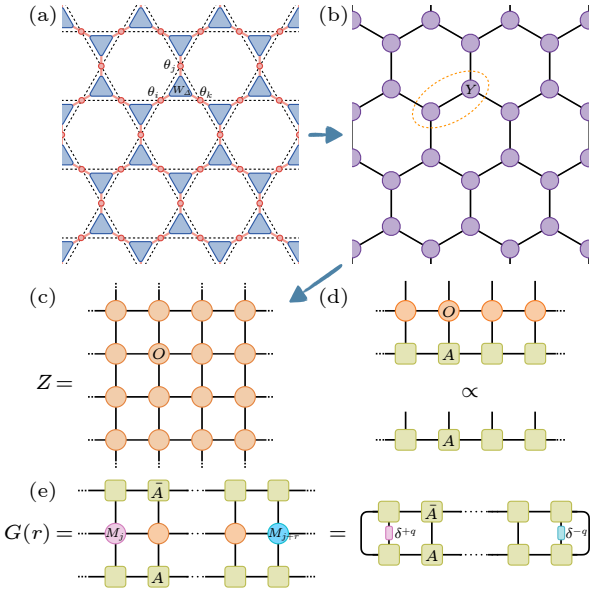

Fig. 3. (a) TN with continuous indices. W tensors represent Boltzmann weights on triangles, and the red dot integrates joint θ variables between two triangles. (b) TN with discrete indices obtained using Fourier transformations. (c) Uniform infinite TN represented by the local tensor O by combining two neighboring Y tensors. (d) Fixed-point MPS eigenequation for the 1D transfer operator. (e) Two-point correlation function calculated by contracting a sequence of channel operators with canonical MPS.

because they do not introduce a phase mismatch on any triangle. In contrast, fractional vortices create a phase mismatch among the six surrounding spins of a hexagon, as shown by the orange line extending from the center of the hexagons in Fig. 2(b), and incur a higher energy cost.

At low temperatures, the AF XY model (2) can be mapped to a 2D Coulomb gas with charges $Q_{\rm h} = \frac{1}{3}\sum_{t=1}^{6}\tau_t + m_{\rm h}$, where $m_{\rm h}$ are integers defined at the hexagon centers.[29] The constraint $\sum_{t=1}^{6}\tau_t \equiv 0 \pmod 6$ ensures that integer vortices can be freely excited at low temperatures, whereas fractional vortices are bound in pairs because of their higher energy costs. As shown in Fig. 2(a), a pair of $\pm\frac{1}{3}$ vortices can be created by switching the chiralities of two adjacent triangles. The fractional vortex pairs were connected by a topological string, along which a phase mismatch of $2\pi/3$ existed. Upon increasing the temperature, these fractional vortices unbound at the BKT transition, indicating the destruction of the QLRO in $\exp(i3\theta)$.

The flux quantization of $\frac{h}{6e}$ arises from the QLRO of $\exp(i3\theta)$, where the SC order parameter is $\Delta_{6e} \propto \Delta_{Q_a}\Delta_{Q_b}\Delta_{Q_c} = \Delta^3\exp(i3\theta)$, describing a six-electron bound state.[20,22] From the minimal coupling relation $\nabla\theta = \frac{6e}{\hbar}\boldsymbol{A}$, integration around a closed-loop enclosing a vortex core yields the flux quantization condition $\Phi_{6e} = \frac{h}{6e}$, corresponding to the 1/3 vortex in the phase field.

TN Methods. The TN approach is particularly well suited for investigating the low-temperature regime of frustrated models because the massive degeneracy induced by strong frustration can be efficiently encoded in local tensors.[34–37] The first step in applying the TN method is to express the partition function of the lattice model (2) as a TN. To account for the chiral DoF associated with each triangle, the partition function is decomposed into a product of the local Boltzmann weights, as shown in Fig. 3(a),

$$Z = \prod_i \int \frac{d\theta_i}{2\pi} \prod_{\Delta} W_{\Delta}, \tag{3}$$

where $W_{\Delta}(\theta_i, \theta_j, \theta_k) = \mathrm{e}^{-\beta H_{\Delta}}$ is a three-leg tensor with continuous $U(1)$ indices, as depicted by the red dots on the lattice sites. The local Hamiltonian $H_{\Delta}(\theta_i, \theta_j, \theta_k)$ for each triangle is defined as $H_{\Delta} = J\sum_{\langle i,j\rangle\in\Delta}\cos(\theta_i - \theta_j)$.

Then, a Fourier transformation is applied to bring the local tensor W_{Δ} onto a discrete basis, as shown in Fig. 3(b),

$$Y_{n_1,n_2,n_3} = \prod_{i=1}^{3}\int \frac{d\theta_i}{2\pi} W_{\Delta}(\theta_1,\theta_2,\theta_3)\mathrm{e}^{\mathrm{i}n_1\theta_1+\mathrm{i}n_2\theta_2+\mathrm{i}n_3\theta_3}. \tag{4}$$

From the saddle point approximation, the asymptotic formula $Y_{n_1,n_2,n_3} \propto \exp[-\frac{1}{3\beta}(n_1^2+n_2^2+n_3^2)]$ can be obtained, implying exponential decay with tensor indices n. Hence, the local Y tensors can be safely truncated using finite bond dimensions. Finally, the translation-invariant local tensor O is obtained by combining a pair of Y tensors $O^{n_3,n_4}_{n_1,n_2} = \sum_{n_5} Y_{n_1,n_2,n_5}Y_{n_3,n_4,n_5}$. The uniform TN representation of the partition function shown in Fig. 3(c) is given by

$$Z = \mathrm{tTr}\prod_s O^{n_3,n_4}_{n_1,n_2}(s), \tag{5}$$

where tTr denotes the tensor contraction over all auxiliary bonds.

In the thermodynamic limit, the fundamental objective of calculating the partition function is the row-to-row transfer matrix $T(\beta) = \mathrm{tTr}[\cdots O(p)O(q)O(r)\cdots]$, which is analogous to the matrix product operator (MPO) in a 1D quantum chain. The contraction of the TN is reduced to obtain the leading eigenvalues and eigenvectors,

$$T(\beta)|\Psi(A)\rangle = \Lambda_{\max}|\Psi(A)\rangle. \tag{6}$$

As shown in Fig. 3(d), $|\Psi(A)\rangle$ is the leading eigenvector represented by the matrix product states (MPS) composed of uniform local A tensors, with an auxiliary bond dimension D that controls the accuracy of the approximation.[43] The fixed-point eigenequation can be solved accurately using the variational uniform matrix product state (VUMPS) algorithm.[43–45]

Once the fixed points are achieved, various physical quantities can be calculated efficiently within the TN framework. The entanglement entropy of the 1D quantum correspondence is obtained directly from the Schmidt decomposition of $|\Psi(A)\rangle$, where $S_{\mathrm{E}} = -\sum_{\alpha=1}^{D} s_\alpha^2 \ln s_\alpha^2$ and s_α are singular values. Local observables are computed by inserting the corresponding impurity tensors into the tensor network for the partition function. For $\mathrm{e}^{\mathrm{i}q\theta_j}$, the impurity tensor modifies the $U(1)$ charge conservation law $\delta_{n_1+n_2+n_3,0}$ in the Y tensor to $\delta_{n_1+n_2+n_3+q,0} = \sum_{n_4} \delta_{n_1+n_2+n_4,0}\delta_{n_3+q,n_4}$, introducing an additional unbalanced delta tensor $\delta^{+q} = \delta_{n_1+q,n_2}$.

Using the MPS fixed point, the contraction of a TN containing impurity tensors is reduced to a trace of an infinite sequence of channel operators, which can be further simplified to the contraction of a smaller network. As shown in Fig. 3(e), the two-point correlation function is given by

$$G_q(r) = \langle \cos(q\theta_i - q\theta_{i+r})\rangle = \langle \mathrm{e}^{\mathrm{i}q\theta_i}\mathrm{e}^{-\mathrm{i}q\theta_{i+r}}\rangle, \tag{7}$$

where the canonical form of MPS is employed to ensure efficient contraction.

Thermodynamic Quantities. The entanglement entropy of the fixed-point MPS for 1D quantum correspondence exhibited singularities at critical temperatures, providing a clear criterion for phase transitions in the thermodynamic limit. As shown in Fig. 4(a), S_{E} displayed a sharp singularity at $T/J \simeq 0.075$, indicating a single-phase transition at a low temperature. The peak position remained almost unchanged for MPS bond dimensions ranging from $D = 80$ to 120, allowing the precise determination of the transition temperature, which agreed well with the theoretical predictions of $T_{\mathrm{c}}/J \approx \frac{\pi/\sqrt{3}}{72}$ for the unbinding temperature of 1/3 vortex pairs.[32] The TN approach enables efficient exploration of the previously inaccessible extremely low-temperature regime. For $D = 100$, S_{E} was calculated at temperatures as low as $T/J = 10^{-5}$ and remained smooth, eliminating the possibility of a transition to long-range chiral order at low temperatures.

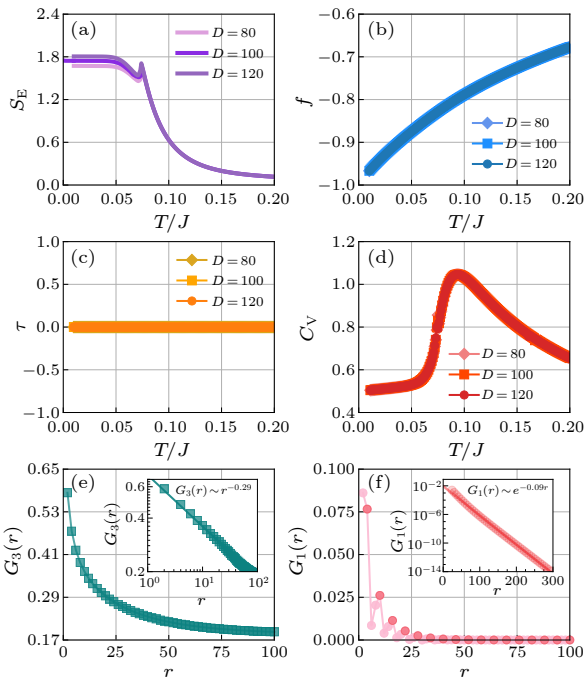

Fig. 4. (a) Entanglement entropy S_{E} as a function of the temperature for different MPS bond dimensions. For $D = 100$, calculations extended to the lowest temperature of $T/J = 10^{-5}$. (b) The free-energy remained smooth across all temperatures, indicating a continuous phase transition. (c) The chirality τ was zero at all temperatures, confirming the absence of long-range chiral order. (d) The specific heat C_{V} exhibited a rounded bump above the critical temperature T_{c}, characteristic of a BKT transition. (e) The correlation function $G_3(r)$ for 1/3 fractional vortices exhibited a power-law decay at $T/J = 0.07$ below T_{c}. (f) The correlation function $G_1(r)$ for integer vortices decayed exponentially at $T/J = 0.07$.

The thermodynamic properties were further investigated to gain insight into the phase transition. The thermodynamic quantities converged well and remained consistent across the different MPS bond dimensions. The free-energy per site was calculated from the eigenvalues of (6) as $f = -\frac{1}{3\beta}\ln\lambda$. As shown in Fig. 4(b), the free energy curve was perfectly smooth, indicating a continuous phase transition. The expected chirality is given by $\tau = \frac{2}{3\sqrt{3}}\sum_{\langle i,j\rangle}\langle \sin(\theta_i - \theta_j)\rangle$. As shown in Fig. 4(c), τ was zero at all temperatures, confirming the absence of long-range chiral order owing to strong chirality fluctuations. Furthermore, $\langle \cos(\theta_i - \theta_j)\rangle \to -1/2$ was observed at low temperatures, implying that the angle between NN spins approached $2\pi/3$. In addition, the specific heat, derived as $C_{\mathrm{V}} = \frac{\mathrm{d}u}{\mathrm{d}T}$, showed a rounded bump around $T/J = 0.095$ as displayed in Fig. 4(d), which was higher than the transition temperature determined from the entanglement entropy. The smooth behavior of the thermodynamic properties eliminated the possibility of first- or second-order transitions due to the lifting of chirality degeneracy, which was consistent with a BKT transition.

Correlation Functions. To investigate the nature of the phase transition, two correlation functions, $G_1(r)$ and $G_3(r)$, were calculated for integer and fractional vortices, as defined in Eq. (7). A comparison of the two correla-

tion functions in the low-temperature phase is shown in Figs. 4(e) and 4(f). At $T/J = 0.07$ below T_c, $G_3(r)$ exhibited a power-law decay with distance, indicating the QLRO of fractional vortices, whereas $G_1(r)$ decayed exponentially, reflecting the absence of LRO for integer vortices. The exponential decay in $e^{i\theta}$ can be attributed to the free fluctuations among different ground-state chirality patterns, where the uncertainty in the phase difference in multiples of $2\pi/3$ increases with distance and destroys the long-range correlations in θ fields. Interestingly, $G_1(r)$ showed damped oscillations in the short-range, but decayed rapidly at larger distances. These oscillations arise because spin-wave fluctuations promote short-range chirality ordering but are too weak to lift the ground-state degeneracy. Above T_c, both $G_1(r)$ and $G_3(r)$ decayed exponentially, signaling that the system transitioned into a disordered phase.

This distinction underscores the contrasting roles of the integer and fractional vortices. At low temperatures, the proliferation of integer vortices disrupts the phase coherence between the charge-2e Cooper pairs. Meanwhile, 1/3 vortex pairs exhibit QLRO below T_c, reflecting the condensation of Cooper sextuples which is a hallmark of charge-6e SC.[18] Above T_c, the system transitioned to the normal phase through a BKT transition driven by the dissociation of the fractional vortices.

Discussion and Conclusion. In this study, the unconventional SC in the Kagome SC CsV_3Sb_5[18] was investigated, focusing on the emergence of charge-6e SC at temperatures higher than the conventional charge-2e SC state. By modeling the phase coherence of the SC order parameter using a frustrated XY model with NN interactions on an emergent Kagome lattice, it was demonstrated that the condensation of fractional vortices with 1/3 vorticity plays a crucial role in stabilizing charge-6e SC. Using state-of-the-art TN methods,[34–37] the nature of this phase transition was clarified. The critical temperature was precisely determined from the entanglement entropy singularity in 1D quantum correspondence. A systematic analysis of the thermodynamic properties and correlation functions in the thermodynamic limit revealed a single BKT transition at $T_c/J \simeq 0.075$ driven by the unbinding of 1/3 fractional vortex-antivortex pairs. Below T_c, the correlation functions for the fractional vortices exhibited a power-law decay, whereas those for the integer vortices decayed exponentially. The absence of chiral long-range order or phase coherence between integer vortices demonstrates that the low-temperature phase is dominated by charge-6e SC with no contribution from charge-2e SC.

It should be noted that the phase transition from charge-2e SC to charge-6e SC was not addressed in this study. Stabilization of the PDW state can be achieved by further incorporating NNN interactions into the AF XY Kagome model, where the destruction of the PDW order is expected to occur via a first-order phase transition.[23,32,46] A full phase diagram, including both NN and NNN interactions, should be the subject of future research. Significant challenges have arisen in its exploration, such as the large bond dimensions required for TN methods and the excessively long relaxation times encountered in Monte Carlo simulations. A systematic study of the complete phase diagram would offer valuable insights into the interplay between interactions and frustration in these systems.

Alternatively, the PDW order could be destabilized by a weak disorder or 2D thermal melting.[19–21,47–49] Further investigation of these possibilities may elucidate unresolved issues, including the origin of the charge-4e oscillations observed in smaller samples.[18] These phenomena, which were not addressed in this study, highlight the need for future theoretical and experimental efforts to better understand the rich physics of Kagome superconductors.

Acknowledgements. The authors are grateful to Yu-Tong Lin for the stimulating discussions. This study was supported by the National Key Research and Development Program of China (Grant No. 2023YFA1406400).

References

[1] Balents L 2010 *Nature* **464** 199
[2] Ortiz B R, Gomes L C, Morey J R, Winiarski M, Bordelon M, Mangum J S, Oswald I W H, Rodriguez-Rivera J A, Neilson J R, Wilson S D, Ertekin E, McQueen T M, and Toberer E S 2019 *Phys. Rev. Mater.* **3** 094407
[3] Broholm C, Cava R J, Kivelson S A, Nocera D G, Norman M R, and Senthil T 2020 *Science* **367** eaay0668
[4] Neupert T, Denner M M, Yin J X, Thomale R, and Hasan M Z 2022 *Nat. Phys.* **18** 137
[5] Jiang K, Wu T, Yin J X, Wang Z, Hasan M Z, Wilson S D, Chen X, and Hu J 2023 *National Science Review* **10** nwac199
[6] Jiang Y X, Yin J X, Denner M M, Shumiya N, Ortiz B R, Xu G, Guguchia Z, He J, Hossain M S, Liu X, Ruff J, Kautzsch L, Zhang S S, Chang G, Belopolski I, Zhang Q, Cochran T A, Multer D, Litskevich M, Cheng Z J, Yang X P, Wang Z, Thomale R, Neupert T, Wilson S D, and Hasan M Z 2021 *Nat. Mater.* **20** 1353
[7] Liang Z, Hou X, Zhang F, Ma W, Wu P, Zhang Z, Yu F, Ying J J, Jiang K, Shan L, Wang Z, and Chen X H 2021 *Phys. Rev. X* **11** 031026
[8] Li X, Zou C, Ding Y, Yan H, Ye S, Li H, Hao Z, Zhao L, Zhou X, and Wang Y 2021 *Phys. Rev. X* **11** 011007
[9] Ortiz B R, Teicher S M L, Kautzsch L, Sarte P M, Ratcliff N, Harter J, Ruff J P C, Seshadri R, and Wilson S D 2021 *Phys. Rev. X* **11** 041030
[10] Luo H, Gao Q, Liu H, Gu Y, Wu D, Yi C, Jia J, Wu S, Luo X, Xu Y, Zhao L, Wang Q, Mao H, Liu G, Zhu Z, Shi Y, Jiang K, Hu J, Xu Z, and Zhou X J 2022 *Nat. Commun.* **13** 273
[11] Hu Y, Wu X, Ortiz B R, Han X, Plumb N C, Wilson S D, Schnyder A P, and Shi M 2022 *Phys. Rev. B* **106** L241106
[12] Kang M, Fang S, Kim J-K, Ortiz B R, Ryu S H, Kim J, Yoo J, Sangiovanni G, Di Sante D, Park B G, Jozwiak C, Bostwick A, Rotenberg E, Kaxiras E, Wilson S D, Park J H, and Comin R 2022 *Nat. Phys.* **18** 301
[13] Nakayama K, Li Y, Kato T, Liu M, Wang Z, Takahashi T, Yao Y, and Sato T 2022 *Phys. Rev. X* **12** 011001
[14] Mielke C, Das D, Yin J X, Liu H, Gupta R, Jiang Y X, Medarde M, Wu X, Lei H C, Chang J, Dai P, Si Q, Miao H, Thomale R, Neupert T, Shi Y, Khasanov R, Hasan M Z, Luetkens H, and Guguchia Z 2022 *Nature* **602** 245
[15] Le T, Pan Z, Xu Z, Liu J, Wang J, Lou Z, Yang X, Wang Z, Yao Y, Wu C, and Lin X 2024 *Nature* **630** 64
[16] Zhao H, Li H, Ortiz B R, Teicher S M L, Park T, Ye M, Wang Z, Balents L, Wilson S D, and Zeljkovic I 2021 *Nature* **599** 216

[17] Chen H, Yang H, Hu B, Zhao Z, Yuan J, Xing Y, Qian G, Huang Z, Li G, Ye Y, Ma S, Ni S, Zhang H, Yin Q, Gong C, Tu Z, Lei H, Tan H, Zhou S, Shen C, Dong X, Yan B, Wang Z, and Gao H J 2021 *Nature* **599** 222

[18] Ge J, Wang P, Xing Y, Yin Q, Wang A, Shen J, Lei H, Wang Z, and Wang J 2024 *Phys. Rev. X* **14** 021025

[19] Agterberg D F and Tsunetsugu H 2008 *Nat. Phys.* **4** 639

[20] Agterberg D F, Geracie M, and Tsunetsugu H 2011 *Phys. Rev. B* **84** 014513

[21] Agterberg D F, Davis J S, Edkins S D, Fradkin E, Van Harlingen D J, Kivelson S A, Lee P A, Radzihovsky L, Tranquada J M, and Wang Y 2020 *Annu. Rev. Condens. Matter Phys.* **11** 231

[22] Zhou S and Wang Z 2022 *Nat. Commun.* **13** 7288

[23] Lin T Y, Song F F, and Zhang G M 2025 *Phys. Rev. B* **111** 054508

[24] Han X, Chen H, Tan H, Cao Z, Huang Z, Ye Y, Zhao Z, Shen C, Yang H, Yan B, Wang Z, and Gao H J 2024 arXiv:2408.06174v1 [cond-mat.supr-con]

[25] Deng H, Qin H, Liu G, Yang T, Fu R, Zhang Z, Wu X, Wang Z, Shi Y, Liu J, Liu H, Yan X Y, Song W, Xu X, Zhao Y, Yi M, Xu G, Hohmann H, Holbæk S C, Dürrnagel M, Zhou S, Chang G, Yao Y, Wang Q, Guguchia Z, Neupert T, Thomale R, Fischer M H, and Yin J X 2024 *Nature* **632** 775

[26] Emery V J and Kivelson S A 1995 *Nature* **374** 434

[27] Carlson E W, Kivelson S A, Emery V J, and Manousakis E 1999 *Phys. Rev. Lett.* **83** 612

[28] Li Q, Hücker M, Gu G D, Tsvelik A M, and Tranquada J M 2007 *Phys. Rev. Lett.* **99** 067001

[29] Rzchowski M S 1997 *Phys. Rev. B* **55** 11745

[30] Park K and Huse D A 2001 *Phys. Rev. B* **64** 134522

[31] Harris A B, Kallin C, and Berlinsky A J 1992 *Phys. Rev. B* **45** 2899

[32] Korshunov S E 2002 *Phys. Rev. B* **65** 054416

[33] Andreanov A and Fistul M V 2020 *Phys. Rev. B* **102** 140405

[34] Vanhecke B, Colbois J, Vanderstraeten L, Verstraete F, and Mila F 2021 *Phys. Rev. Res.* **3** 013041

[35] Song F F and Zhang G M 2022 *Phys. Rev. B* **105** 134516

[36] Song F F and Zhang G M 2023 *Phys. Rev. B* **108** 014424

[37] Song F F, Lin T Y, and Zhang G M 2023 *Phys. Rev. B* **108** 224404

[38] Berezinsky V L 1971 *Sov. Phys. JETP* **32** 493

[39] Kosterlitz J M and Thouless D J 1973 *J. Phys. C: Solid State Phys.* **6** 1181

[40] Kosterlitz J M 1974 *J. Phys. C: Solid State Phys.* **7** 1046

[41] Huse D A and Rutenberg A D 1992 *Phys. Rev. B* **45** 7536

[42] Korshunov S E and Uimin G V 1986 *J. Stat. Phys.* **43** 1

[43] Zauner-Stauber V, Vanderstraeten L, Fishman M T, Verstraete F, and Haegeman J 2018 *Phys. Rev. B* **97** 045145

[44] Vanderstraeten L, Vanhecke B, Läuchli A M, and Verstraete F 2019 *Phys. Rev. E* **100** 062136

[45] Nietner A, Vanhecke B, Verstraete F, Eisert J, and Vanderstraeten L 2020 *Quantum* **4** 328

[46] Kakizawa F, Misawa T, and Shinaoka H 2024 *Phys. Rev. B* **109** 014439

[47] Nelson D R 1978 *Phys. Rev. B* **18** 2318

[48] Nelson D R and Halperin B I 1979 *Phys. Rev. B* **19** 2457

[49] Young A P 1979 *Phys. Rev. B* **19** 1855